

NJC

Accepted Manuscript



This is an *Accepted Manuscript*, which has been through the Royal Society of Chemistry peer review process and has been accepted for publication.

Accepted Manuscripts are published online shortly after acceptance, before technical editing, formatting and proof reading. Using this free service, authors can make their results available to the community, in citable form, before we publish the edited article. We will replace this *Accepted Manuscript* with the edited and formatted *Advance Article* as soon as it is available.

You can find more information about *Accepted Manuscripts* in the [Information for Authors](#).

Please note that technical editing may introduce minor changes to the text and/or graphics, which may alter content. The journal's standard [Terms & Conditions](#) and the [Ethical guidelines](#) still apply. In no event shall the Royal Society of Chemistry be held responsible for any errors or omissions in this *Accepted Manuscript* or any consequences arising from the use of any information it contains.



www.rsc.org/njc

Enhanced thermal stability and lifetime of epoxy nanocomposites using covalently functionalized clay: Experimental and modelling

Omid Zabihi, Hamid Khayyam, Bronwyn Fox, Minoo Naebe*

Institute for Frontier Materials, Deakin University, Geelong, Victoria, Australia

Abstract:

The presented work aims at finding a relationship between kinetic model of thermal degradation process with the physiochemical structure of epoxy/clay nanocomposites in order to understand its service temperature. In this work, two different types of modified clay including clay modified with (3-aminopropyl)triethoxysilane (APTES) and a commercial organoclay were covalently and non-covalently incorporated into epoxy matrix, respectively. The effect of different concentrations of silanized clay on thermal behaviour of epoxy nanocomposites were firstly investigated in order to choose the optimum clay concentration. Afterwards, thermal characteristics of degradation process of epoxy nanocomposites were obtained by TGA analysis and the results were employed to determine the kinetic parameters using model-free isoconversional and model-fitting methods. The obtained kinetic parameters were used to model the whole degradation process. The results showed that the incorporation of the different modified clay into epoxy matrix change the mathematical model of degradation process, associating with different orientations of clay into epoxy matrix confirming by XRD results. The obtained models for each epoxy nanocomposite systems were used to investigate the dependence of degradation rate and degradation time on temperature and conversion degree. Our results provide an explanation as to how the life time of epoxy and its nanocomposites change in a wide range of operating temperatures as a result of their structural changes.

Keywords: Thermal durability, Solid state degradation; Epoxy polymers; Clay; Nanocomposites

*Corresponding author: Tel: +61469570372

E-mail: minoo.naebe@deakin.edu.au

1. Introduction

Knowledge concerning long-term behavior of high-performance polymers usually takes into account the first requirements for their industrial applications in high temperature environments. Thus, the decomposition study of polymers is of momentous because it can characterize the upper temperature limit and the lifetime of the system¹⁻³. Modelling has extensively become an essential tool for engineers to predict the thermal durability of their materials before employing them in their industrial process, which leads to significant reduction in product development costs^{4,5}. Nowadays, competitive market needs to optimize manufacturing cost, time, and quality. To do these, manufacturers should control and predict variability of any product which relate to the desired outputs⁴. Therefore, an accurate model which relates process variables and desired outputs needs to be developed. Modeling is imperative since it enables us to understand the product behavior and determine the optimum operating conditions of the product for a high yield, low cost, robust operation, and life time quality⁶. The thermal degradation and decomposition of polymer nanocomposites are always a complex topic that involves the combined effects of thermal, chemical and physical processes. In order to track the thermal events occur during the degradation process, mechanistic studies on involving reactions are not usually feasible. Therefore, phenomenological studies are then preferred to investigate the complex process of degradation^{7,8}. In fact, following up thermal events occurred during degradation process using TGA analysis can be used to effectively simulate the thermal conditions in an industrial environment at which a polymer composite is exposed to high temperatures. Typically, modeling based on advanced kinetic analysis can provide reliable predictions on thermal events of degradation process.

Due to light weight, low cost, high strength, and easy processing epoxy nanocomposites are used for different applications in various industries⁹⁻¹¹. The growing use of thermosetting epoxy nanocomposites requires knowledge of their thermal properties in high temperatures to ensure proper performance. When epoxy polymers are exposed to high temperatures the organic matrix decomposes with the release of corrosion smoke, heat and toxic dust.¹²⁻¹⁴. Therefore, it is necessary to improve thermal durability along with its mechanical and physical properties. Polymeric composites reinforced with layered silicates has extensively received increasing attention due to the having the improved properties in terms of modulus^{15,16}, toughness¹⁷, fire resistance^{18,19}, and dimensional stability^{10,20}. However, the intrinsic hydrophilicity of clay makes its uniform dispersibility into epoxy matrix highly difficult²¹. Therefore, to improve their interfacial interaction, modification of the clay by organophilic

materials is inevitable. The effect of different organic modifiers on the mechanical and physical properties as well as thermal stability of epoxy polymers has been widely reported²²⁻³⁰.

Despite the extensive literatures on the thermal and mechanical properties of modified clay/epoxy nanocomposites, detailed studies on the effects of surface modified clay on change of mechanism of degradation process of epoxy nanocomposites in relation with its structures are generally not available. Besides, to the best of our knowledge there is not any report in literature on prediction of thermal durability during degradation using kinetically modelling of the epoxy degradation process. The aim of this study is to kinetically investigate thermal degradation process of epoxy nanocomposites containing different types of modified clay and to obtain its kinetic parameters. Knowing kinetic parameters, thermal behavior during degradation can be described as a phenomenological process instead of mechanistic investigation. For this purpose, the effect of different surface modifications of clay on degradation process was studied in order to understand the influence of physiochemical structure of epoxy nanocomposites on degradation process. The main objective is to obtain an insight into the effect of different structures and orientations of clay on mechanism of thermal degradation process as well as thermal durability of epoxy systems.

2. Experimental

2.1. Materials

diglycidyl ether of bisphenol A (D.E.R 332) from Sigma Aldrich with an epoxy equivalent weight of 175 gr eq⁻¹ was used as epoxy polymer. Isophorone-diamine and (3-aminopropyl)triethoxysilane were purchased from Sigma and used as received. The pristine clay is the sodium montmorillonite and the organoclay is a commercial product under the name of Nanomer I.28E containing 25-30 wt% trimethyl stearyl ammonium, which were supplied by Nanocor Co., USA. All solvents used in this study were of analytical grade.

2.2. Silanization of clay

Silanized clay was prepared according to the “slurry-compounding” process with some modifications²⁴. Typically, specific amounts of pristine clay were dispersed into 200 mL of DI water to form a fine suspension, which was stirred for 2 h and sonicated for 1 h. The suspension was poured into 200 mL of acetone and stirred again for 1 h. The precipitate was filtered and washed with acetone. The wet product was added to 50 mL of acetone to form slurry. Then, 30% wt of (3-aminopropyl)triethoxysilane (APTES) with respect to the pristine clay was added into the slurry. The slurry was refluxed for 18 h at 70 °C and sonicated for 1

h. To determine the grafting yield of APTES into clay, slurry containing silanized clay was evaporated under vacuum and dried for 24 h at 70 °C to obtain the silanized clay (s-clay).

2.3. Epoxy nanocomposites preparation

To prepare the epoxy nanocomposites containing silanized clay, the slurry was mixed with specific quantities of epoxy resin and mechanically stirred for 2 h at 60 °C and sonicated for 30 min. In a series of experiments, the amount of silanized clay was chosen to be 0, 0.5, 1, 2, 5 and 10% of the total mass of the compositions and then acetone was evaporated by drying in a vacuum oven for 24 h. Bulk samples of 1 g were prepared and kept in a refrigerator prior to the DSC measurements. For the TGA and XRD experiments, a stoichiometric quantity of the isophorone-diamine as curing agent was added and the mixture was stirred for 30 min at room temperature and then degassed under vacuum for 1 h. Finally, the mixture was cured at 75 °C for 6 h and postcured at 120 °C for 1 h. Hereafter, the nanocomposites prepared using the slurry-compounding process are designated as epoxy/s-clay systems. Epoxy nanocomposite containing commercial organoclay was prepared according to the procedure below. 2% wt commercial modified organoclay (o-clay) was added to the mixture of epoxy resin and then mechanically stirred for 2 h at 60 °C and sonicated for 30 min. Afterwards, the same procedure mentioned above was applied to cure these epoxy systems which are designated as epoxy/o-clay systems.

2.4. Measurements

FTIR spectra were recorded by a FTIR spectrophotometer (Bruker Optics) using the KBr method. Thermogravimetric analyses were carried out using Perkin–Elmer TGA in the temperature range from 30 to 750 °C at the heating rate 10 °C min⁻¹ under nitrogen atmosphere in order to evaluate the grafting yield of APTES into clay. DSC measurements were performed using TA Q200 DSC in high purity nitrogen atmosphere. The samples were heated in the temperature range of 25 to 300 °C at the heating rate of 10 °C min⁻¹. Each sample in the DSC experiments was repeated three times and averaged to be used for further analysis. From the exotherms obtained, the heat of reaction and the peak temperature were also determined. A re-scan treatment at low heating rate of 2 °C min⁻¹ was used to estimate the glass transition temperature. TGA tests of epoxy nanocomposites were operated in a dynamic mode and the temperature range of the experiments was between 25 to 750 °C at the heating rates of 5, 10, 15, and 20 °C min⁻¹. The sample mass was about 20 mg. XRD patterns were obtained using a PANalytical X'Pert Pro Diffractometer with Cu K α radiation ($\lambda=1.54184$ Å), which was operated at 45 kV and 40 mA. Scans were acquired in continuous mode over a range of 2°–10° (2 θ) with a step size of 0.033.

2.5. Theoretical background

The primary purpose of the kinetic analysis is to obtain the kinetic triplet including activation energy (E), pre-exponential factor (A), and process model ($f(\alpha)$). Recently, ICTAC Kinetics Committee has reviewed the relationship between the theoretical degradation process and their mathematical models^{31, 32}. Generally, the rate of a solid-state process can be generally expressed by:

$$\text{Rate} = \frac{d\alpha}{dt} = Af(\alpha)e^{-\frac{E}{RT}} \quad (1)$$

where T is absolute temperature, R is the gas constant, and α is the conversion degree. Table S1 shows the most frequency used models for polymers according to the recommendations of ICTAC Kinetics Committee³². For TG measurements, α is defined by:

$$\alpha = \frac{m_0 - m_i}{m_0 - m_f} \quad (2)$$

where m_0 , m_f and m_i are initial, final and current sample mass at temperature T , respectively.

If the temperature of the sample is changed by a controlled and constant heating rate, $\beta = dT/dt$, the variation in the degree of conversion could be analyzed as a function of temperature. This temperature will be dependent on the time of heating. Therefore, the reaction rate might be explained as:

$$\frac{d\alpha}{dT} = \frac{A}{\beta} e^{-\frac{E}{RT}} f(\alpha) \quad (3)$$

Integration of Eq. 3 from an initial temperature corresponding to a null degree of conversion (T_0) to the temperature corresponding to its conversion (T_α) gives³²:

$$g(\alpha) = \frac{A}{\beta} \int_0^{T_\alpha} e^{-\frac{E}{RT}} dT \quad (4)$$

where $g(\alpha)$ is the integral form of the reaction model ($g(\alpha) = \int_0^\alpha [f(\alpha)]^{-1} d\alpha$) and right side of Eq. 4 is known as Arrhenius integral or the temperature integral that has no analytical solution but can be estimated by numerical methods³³. The temperature integral

$$I(E, T) = \int_0^{T_\alpha} \exp\left(\frac{E}{RT}\right) dT \quad (5)$$

is determined by the Senum-Yang approximation, which gives errors lower than 10⁻⁵% for $x=20$ ³⁴:

$$I(E, T) = T e^{\frac{-E}{RT}} \pi(x) \quad (6)$$

where $x = E/RT$ and $\pi(x)$ is as follows:

$$\pi(x) = \frac{x^4 + 18x^3 + 86x^2 + 96x}{x^4 + 20x^3 + 120x^2 + 240x + 120} \quad (7)$$

Combination of Eqs. 5 and 6 with Eq. 3 gives:

$$g(\alpha) = \frac{A}{\beta} T. e^{-\frac{E}{RT}}. \pi(x) \quad (8)$$

3. Results and Discussion

3.1. Functionalization of clay

In order to confirm the interaction of APTES with pristine clay, FTIR experiments were performed. Fig.1 shows FTIR spectra of pristine clay and silanized clay as well as pure APTES. As shown in Fig.1 and according to APTES molecular structure, FTIR characteristic peaks for pure APTES are N-H stretching, C-H stretching as well as C-O, Si-C and Si-O bands. The FT-IR spectrum of pristine clay shows -OH stretching frequencies at 3620 cm^{-1} , and broad bands at 3420 and 1635 cm^{-1} can be attributed to adsorbed water molecules. The strong broad band in the range of $900\text{-}1100 \text{ cm}^{-1}$ is related to Si-O bonds. The spectrum of silanized clay displays the same pattern as that of pristine clay, except for some new bands appeared at 2950 cm^{-1} and 2880 cm^{-1} that are attributed to the C-H asymmetric and symmetric stretching of methyl group which confirms successful reaction between APTES and clay. Moreover, peaks of 3300 cm^{-1} , 700 cm^{-1} and 1440 cm^{-1} that respectively corresponds to the N-H stretching, -CH bending vibrations and Si-C stretching further supports the covalent bonding of APTES onto clay, which are also observed in FTIR spectrum of pure APTES.

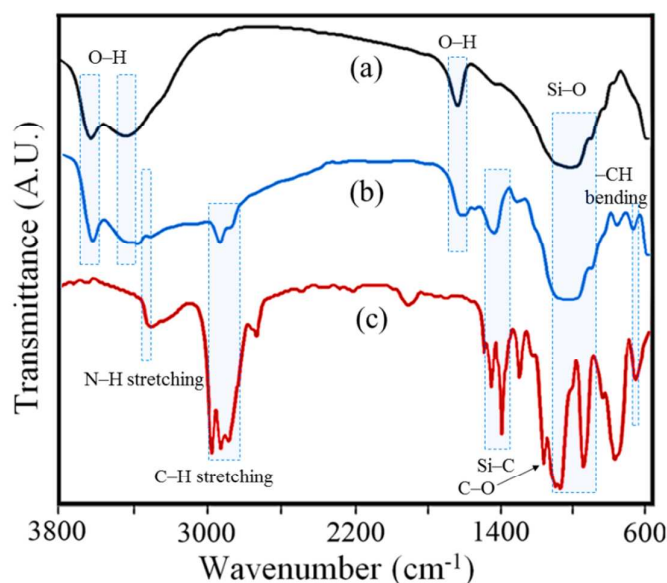


Fig.1. FT-IR spectra of pristine clay (a), s-clay (b) and pure APTES (c).

For better comparison of covalent bonding of APTES onto clay with non-covalent modification of clay, a commercial modified clay was selected. Most commercial modified clays have been prepared according to the ion exchange or electrostatic interaction between modifiers with clay, which are very weak bonds compared to covalent bonds^{28, 29}. Fig. 2 compares the dispersibility of s-clay and o-clay with respect to pristine clay in a biphasic solvent of chloroform/water. The pristine clay has a strong hydrophilic inherent which is obvious in the Fig. 2a. After silanization of clay, covalently grafted APTES which has an organophilic inherent leads to pulling down the clay into the organophilic phase (chloroform) instead of remaining into the hydrophilic phase (water). Moreover, after mixing o-clay with the solvent, it was observed that its organo-modifier is dissolved in organophilic phase while clay remains in hydrophilic phase. This relies on the fact that interaction between organo-modifier with clay is not as strong as interaction between APTES with clay because of its non-covalent bonds. In other words, the presence of the s-clay in the organophilic phase despite the hydrophilic nature of clay denotes strong attachment of APTES to clay so that the organophilic nature of s-clay system outweighs its hydrophilic nature.

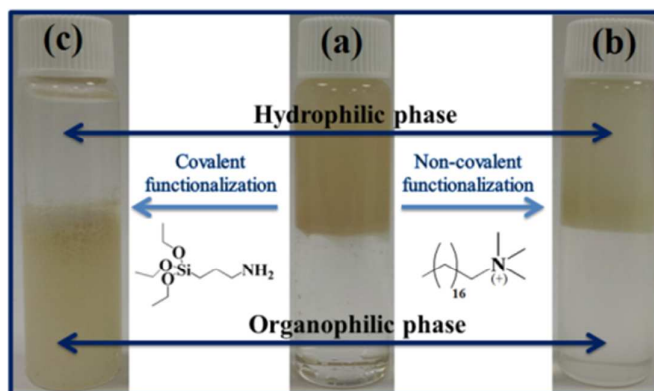


Fig. 2. Solubility profile of pristine clay (a), and o-clay (b), and s-clay (c) in chloroform/water biphasic after 10 min ultrasonication.

TGA was performed on the samples to obtain an estimation of grafting yield of APTES into pristine clay. Typically, the amount of grafted APTES can be calculated using the following equation^{35, 36}:

$$\text{Grafted amount (mequiv/g)} = \frac{1000\Delta W}{(100 - \Delta W)M} \quad (9)$$

where ΔW is percent of weight loss between 200 to 600 °C and M is the molecular weight of APTES. The pristine clay shows around 10% weight loss up to 750 °C which can be assigned to the loss of moisture and hydroxyl groups of clay whereas 25% of silanized clay is degraded at 750 °C (See Fig S.1). The weight loss between 200 °C and 600 °C is 17.24%. Using Eq. 9, the grafted amount of APTES was calculated to be 0.94 mequiv/gr of pristine

clay. The grafting yield of silanization process can be calculated given that the used initial concentration of APTES in preparation of silanized clay is 3 gr per 10 grams of pristine clay. Therefore, grafting yield of APTES into clay is 69.30%. The amount and grafting yield of APTES is slightly higher than that of reported in previous studies³⁵, which can be attributed to the longer time and higher temperature of silanization process, which suggests that the performed surface modifications on “slurry-compounding” process were completely effective to improve the grafting yield.

3.2. Optimized epoxy nanocomposite

The first stage of this study involves determination of the optimum concentration of s-clay to prepare the epoxy nanocomposites. With this aim, DSC and TGA experiments using different percentages of s-clay (0, 0.5, 1, 2, 5 and 15%) were carried out (See supporting information, Figs. S2-S4). Table 1 summarizes the obtained thermal data for different concentration of s-clay. Generally, the total heat of reaction (ΔH_T) of curing of epoxy resin is associated with the epoxy groups and the amine groups of curing agent. With addition of s-clay into epoxy resin, two competitive factors come into play and influence the ΔH_T . The first factor is the presence of amine groups of grafted APTES of s-clay which contribute in the ring opening of epoxy groups, resulting in increase of ΔH_T . The second factor involves the effect of thermal barrier of clay on forming the epoxy matrix, which has been well established in literature³⁷⁻³⁹. As it can be seen, lower levels of s-clay up to 2% significantly increase the ΔH_T of curing of epoxy nanocomposites due to the fact that the contribution of the APTES amine groups is more effective than the barrier effects of clay. At higher concentrations (i.e. 5 and 10%), the barrier effects outweigh the heat generated by the reaction of APTES amine groups with epoxy rings therefore beyond 2% concentration, ΔH_T decrease dramatically. In fact, concentration of 2% is in a balance between producing the additional heat of reaction and thermal barrier effects. The trend of changes of peak temperature of the curing reaction (T_p) also supports our observations that for concentrations higher than 2%, the T_p decreases due to increase in the presence of amine groups upon increase in clay concentration. In other words, curing reaction in the presence of high concentrations of s-clay begins in lower temperatures but with lower ΔH_T which demonstrates that some epoxy groups may have not undergone the curing reaction and consequently the epoxy matrix is not fully cured. Moreover, as it shown in Table 1, the glass transition temperature (T_g) of the cured epoxy nanocomposites are higher than that of the pure epoxy system and its value constantly increases up to concentration of 2% and beyond it decreases. It may be implied that at high levels of the s-clay, the crosslink density will decrease owing to aggregation of clay and topological restrictions resulting in lower

values of reaction heat as discussed above. The increase in T_g of the epoxy nanocomposites containing low levels of s-clay with respect to the pure epoxy could be attributed to the decreased mobility of chain segments of epoxy resins because of the strong interaction of APTES amine groups clay with epoxy matrix with no topological restrictions. The increase in T_g with increasing s-clay loading up to 2% indicates that the mobility of the polymer chains has been reduced after introducing s-clay into the epoxy matrix, suggesting strong interfacial interactions could exist between s-clay and polymer molecules. Moreover, the increase in T_g with increasing in loading of s-clay up to 2% can be attributed to more covalent bonds between amine groups on the s-clay with epoxy polymer that is due to the substantial differences in the dispersion degree of low levels of s-clay compared to the higher levels of s-clay.

Table 1. TGA and DSC measurements on the epoxy nanocomposites having different values of s-clay.

Characterization S-clay (%)	DSC Results			TGA Results	
	ΔH_T (J g ⁻¹)	T_p (°C)	T_g (°C)	$T_{initial}$ (°C)	T_{max} (°C)
0	210±4.5	128.5±0.42	127.5±0.42	339.3	360.1
0.5	215±4.3	131.2±0.02	130.2±0.36	348.5	360.4
1	218±2.5	131.5±0.11	131.3±0.10	352.1	361.6
2	220±3.6	131.8±0.32	132.2±0.53	356.2	368.3
5	190±1.2	135.7±0.42	124.1±0.32	363.0	362.4
10	195±7.2	138.8±0.42	115.4±0.34	365.4	361.7

To better understand the relation between DSC characteristics and thermal stability using TGA data, it is important to prove the effect of different loadings of s-clay on thermal stability of cured epoxy nanocomposites. As it can be seen from Table 1, there is a constant increasing trend in the temperature correspond to 5% weight loss, $T_{initial}$, with increasing the concentration of s-clay which is rationally related to thermal barrier effects of s-clay. Therefore, $T_{initial}$ cannot be meaningfully considered as a comparative factor to evaluate the interaction of clay with epoxy matrix. Instead of $T_{initial}$, temperature corresponding to the maximum of TGA derivative, T_{max} , is considered as a substantial criterion, stemming from the type of interaction between s-clay and polymer chains as well as dispersion of s-clay into polymer matrix. Therefore, as it shown, maximum of T_{max} belongs to the concentration of 2% s-clay. From the thermal analysis data, it can be concluded that the best thermal properties is when 2% s-clay is incorporated into the epoxy matrix.

3.3. Thermal stability assessment

The TGA data of the pure epoxy, epoxy/s-clay, and epoxy/o-clay were obtained at four different heating rates of 5, 10, 15, and 20 °C min⁻¹. Fig. S5 exhibits the curves of weight loss against temperature at various heating rates for these systems. The TGA curves were

analyzed by defining two parameters such as T_{initial} and T_{max} . The results of TGA analysis are shown in Table 2. As it can be seen, epoxy/s-clay system has higher T_{initial} and T_{max} rather than the epoxy/o-clay and pure epoxy systems. The plots of conversion and degradation rate versus temperature for all three epoxy systems were generated in Fig. 3. It shows that a specific conversion for epoxy/s-clay occurs in higher temperature rather than the other epoxy systems. Moreover, the epoxy/s-clay has the lower degradation rate in its T_{max} rather than the epoxy/o-clay and pure epoxy systems.

Table 2. TGA data of the thermal degradation at different heating rates.

Heating rate (°C/min)	Pure epoxy		Epoxy/s-clay		Epoxy/o-clay	
	T_{initial} (°C)	T_{max} (°C)	T_{initial} (°C)	T_{max} (°C)	T_{initial} (°C)	T_{max} (°C)
5	324.4	347.2	337.1	358.5	326.7	355.2
10	339.3	360.1	356.2	368.3	342.5	366.1
15	345.0	368.0	359.6	377.1	347.2	373.3
20	349.4	378.3	362.4	382.4	352.1	379.6

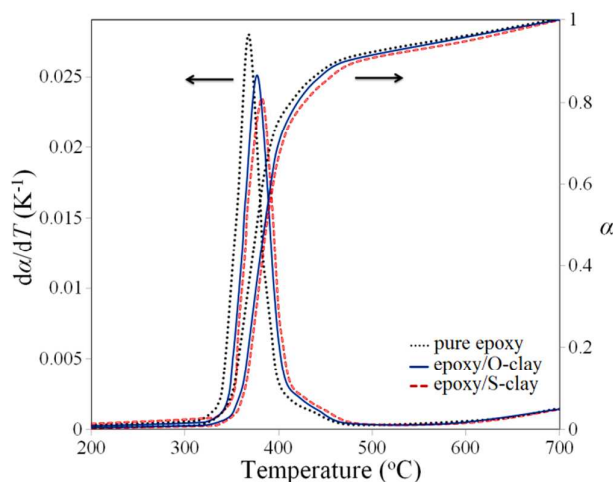


Fig. 3. Plots of $d\alpha/dT$ and α as a function temperature for the thermal degradation of the epoxy systems at the heating rate of 20 °C/min.

To remove the effect of heating rates on thermal degradation, T_{max} was taken for quantitative analysis. Fig. 4 presents dependency of T_{max} on heating rate for epoxy systems. The correlation between T_{max} and heating rate could be expressed as the following equation⁴⁰:

$$T_{\text{max}} = r\beta + T_{\text{max}}^0 \quad (10)$$

where T_{max}^0 is the equilibrium peak thermal degradation temperature by assuming that the heating rate equals 0 °C min⁻¹ and r is the rate constant. As it shown in Fig. 3, T_{max}^0 of filled epoxy systems with clay are higher than that of the pure epoxy, indicating that the presence of clay increases the thermal stability of the composite. However, thermal stability of epoxy/s-clay is higher than that of the epoxy/o-clay. To gain more insights about the comparison of thermal stability of epoxy systems, Kissinger method⁴¹ was utilized in order

to obtain the overall activation energy for the whole thermal degradation process, since it is independent of any pre-assumption about the thermal degradation mechanism. This method relates the logarithm of $\frac{\beta}{T_{max}^2}$ with the inverse of T_{max} according to the following equation:

$$\ln\left(\frac{\beta}{T_{max}^2}\right) = \ln\left(\frac{AR}{E}\right) - \frac{E}{RT_{max}} \quad (11)$$

Plotting $\ln\left(\frac{\beta}{T_{max}^2}\right)$ versus $\frac{1000}{T_{max}}$ gives a straight line from which the E value can be determined using the slope. Fig. 4 presents the Kissinger plots for epoxy systems and then E value for each system was calculated and collected in Table 3. As it can be seen from Table 3, the same trend of thermal stability discussed above is observed for the obtained E values of epoxy systems.

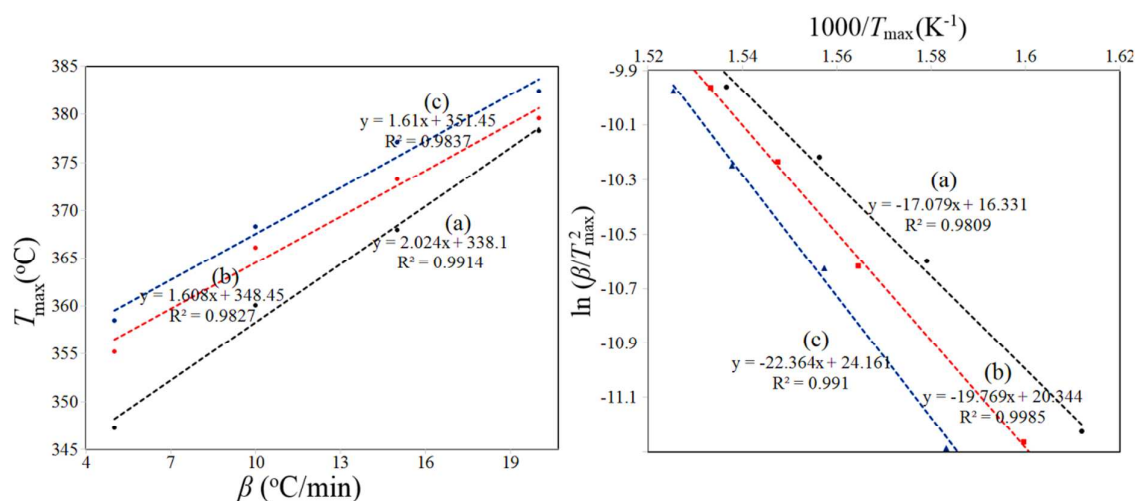


Fig. 4. The plots of T_{max} versus heating rates (left) and Kissinger plots (right) for the pure epoxy (a), epoxy/o-clay (b), and epoxy/s-clay (c) systems.

Table 3. Kinetic parameters obtained from TGA analysis for epoxy systems.

System	E (kJ/mol) (Kissinger)	Mean values of E (kJ/mol) (Friedman)	$\log A$	$f(\alpha)$
Pure epoxy	141.9	144.0	11.36	$3(1-\alpha) [-\ln(1-\alpha)]^{2/3}$
Epoxy/o-clay	164.3	161.1	13.75	$2(1-\alpha)^{1/2}$
Epoxy/s-clay	185.9	189.9	13.17	$3(1-\alpha)^{2/3}$

3.4. Degradation process modeling

According to Eq. 1, in order to model the thermal events during degradation of epoxy, it is required to determine the accurate values of E , A and $f(\alpha)$, so-called triple kinetic analysis³¹. The isoconversional methods to obtain the E value aims to untangle complex and macroscopic kinetics into a specific kinetics as a function of the degree of conversion. It states that at a constant extent of conversion, the reaction rate is a function of temperature only. Therefore, the isoconversional methods require performing a series of experiments at

different heating rates and yield the values of effective E as a function of conversion. Analysis of the resulting E dependence could provide important information about changes in the reaction mechanism as a part of whole phenomenological process, which is described mathematically by $f(\alpha)$. Rearrangement of Eq. 3 leads to the following equation, which calls Friedman method ⁴²:

$$\ln(\beta_i \frac{d\alpha}{dT})_{\alpha,i} = \ln[A_\alpha f(\alpha)] - (\frac{E_\alpha}{RT_{\alpha,i}}) \quad (12)$$

The E corresponding to each α (E_α) is determined from the slope of the plot of $\ln[\beta_i(d\alpha/dT)_{\alpha,i}]$ versus $1/T_\alpha$, at a constant α value. Subscript i is the ordinal number of an experiment performed at a given heating rate. This method is rather accurate because it does not include any mathematical approximations. The dependence of the obtained activation energies by Friedman method on different conversions for three epoxy systems were shown in Fig. 5 and its values along with the mean values are presented in Table 2S and Table 3, respectively. As it can be seen from Fig. 5, values of E_α are quasi-constant up to $\alpha < 0.25$ for both filled epoxy systems while in the pure epoxy system this quasi-constant remains by the end of degradation process. At $0.50 > \alpha > 0.25$, values of E_α of both filled epoxy systems show a sudden increasing trend, attributing to the presence of the organized clay structures which can hinder the chemical bonds breakage. Moreover, it shows that breaking the chemical bonds in presence of s-clay due to the covalent bonds of s-clay into polymer matrix requires more activation energies compared to o-clay. Beyond $\alpha > 0.50$, E_α decreases indicating that the organization and chemical bonds are successively losing and less activation energies are required for residual degradation process. Generally, these dependencies of activation energy on each conversion will be used for determination of kinetic model because it was independent of any preconception regarding the physico-chemical degradation process.

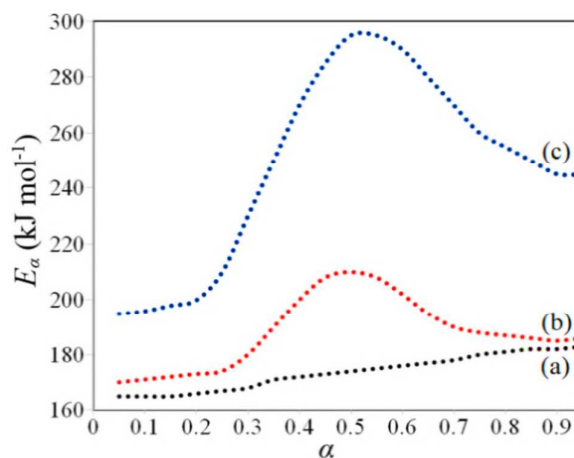


Fig. 5. Dependence of E_α on α for the pure epoxy (a), epoxy/o-clay (b), and epoxy/s-clay (c) systems using Friedman method.

If the activation energy value for each conversion is known the kinetic model of the process can be found using the model-fitting methods. The physico-chemical conversion function of degradation process ($f(\alpha)$) can be determined by using master-plot method proposed by Criado et al.^{31, 43, 44}. Master plots are reference theoretical curves depending on the kinetic model but completely independent of the kinetic parameters of the process. The master-plot method is based on the comparison of theoretical master plots, which are obtained for a wide range of ideal kinetic models, with the experimental master plots^{31, 45}. Applying this method could be led to select the appropriate conversion model for the solid-state process investigated.

By combining the Eqs. 1 and 9, an alternative kinetic equation is obtained:

$$\frac{d\alpha}{dt} = \frac{\beta}{T_{\alpha}\pi(x_{\alpha})} f(\alpha) \cdot g(\alpha) \quad (13)$$

After rearranging the Eq. 13, the $z(\alpha)$ function is defined as:

$$z(\alpha) = [f(\alpha) \cdot g(\alpha)]_{\text{theoretical}} = \left[\left(\frac{d\alpha}{dt} \right)_{\alpha} \frac{T_{\alpha}}{\beta} \pi(x_{\alpha}) \right]_{\text{experimental}} \quad (14)$$

This equation can be used to obtain the master curves as a function of the conversion corresponding to the different models listed in Table S1. By comparison of the theoretical master plots with the experimental master plot, phenomenological model of degradation process can be easily and precisely determined. The master curve plots of $z(\alpha)$ versus α for different mechanisms according to the Criado method have been illustrated in Fig. 6. It clearly shows that the experimental data of $z(\alpha)$ of pure epoxy, epoxy/s-clay and epoxy/o-clay have best fitting with the A_3 , R_3 and R_2 master curves, respectively. The mathematical expression of the obtained models was listed in Table 3. In the case of pure epoxy, the obtained model is in agreement with the previous reports, in which A_n models have been determined as a model for thermal degradation process⁴⁶ and there is not any report to compare the obtained results for the epoxy nanocomposites containing clay. The R_n models are physically considered as phase boundary controlled process models which mean that the degradation process occurs rapidly on the surface of the polymer. The process then advances inward, and the rate of degradation is controlled by the resulting reaction interface progress toward the centre of the polymer. This is attributed to the thermal barrier effect of clay on polymer matrix in such a way that permeation of the heat through the layered structures of epoxy nanocomposites into the center of polymer matrix could be considered as the rate-limiting step.

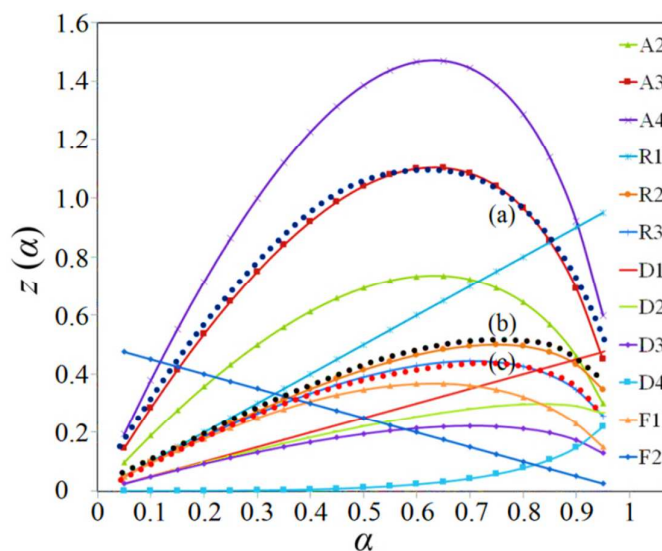


Fig. 6. Comparison of master plots (lines) with experimental data (circles) for the pure epoxy (a), epoxy/o-clay (b), and epoxy/s-clay (c) systems.

XRD data of epoxy nanocomposites can provide information regarding the dispersion type of clay nanostructure into epoxy matrix, which would be used to describe the degradation process. Fig. 7 demonstrates XRD diffractograms of pure epoxy and its nanocomposites. As it shown, pure epoxy and epoxy/s-clay show no peaks in their XRD patterns while epoxy/o-clay exhibits (001) and (002) basal peaks reflection at around 3° and 5° (2θ), which are in agreement with literature²². The direct comparison between the epoxy/o-clay and epoxy/s-clay shows that the exfoliated clay structures into epoxy matrix can be achieved by using s-clay (absence of XRD peaks due to nanolayers disordering) in contrast to the o-clay which induces the formation of a highly ordered intercalated structure. Theoretically, the r values in Eq. 10 imply thermal diffusion rate into epoxy matrix, affected by thermal barrier properties resulting from type of dispersion of clay within epoxy matrix. As is shown, the epoxy/o-clay has the lower r value rather than epoxy/s-clay, indicating the heat diffusion within epoxy/o-clay is more difficult than the epoxy/s-clay. This finding is in agreement with order of R_n models for the filled epoxy nanocomposites so that the order of R_n model in the epoxy/o-clay becomes lower due to the more difficulty in heat diffusion within epoxy/o-clay compared to that of epoxy/s-clay. The order of mathematical model is important due to the fact that increasing the order leads to increasing the degradation rate; however, other kinetic parameters also affect the degradation process rate. Based on the XRD results, Fig. 8 schematically presents the intercalated and exfoliated epoxy systems and its relation with type permeation of the heat into matrix, which affects the degradation process.

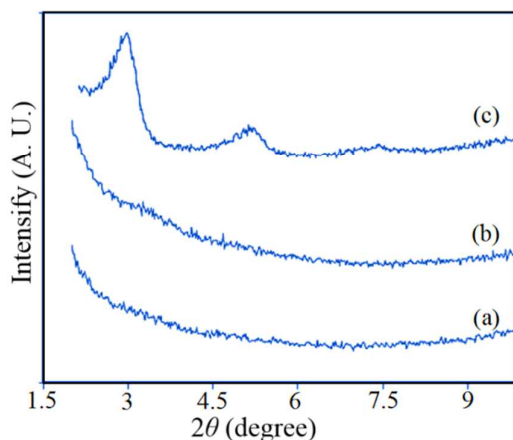


Fig. 7. XRD diffractograms of pure epoxy (a), epoxy/s-nanoclay (b) and epoxy/o-nanoclay (c) systems.

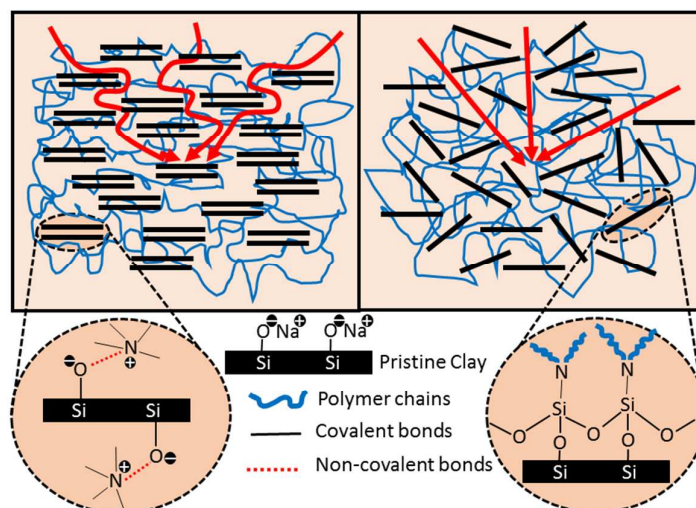


Fig. 8. Ideal scheme of degradation process propagation into the center of epoxy/o-clay (left) and epoxy/s-clay (right) systems considering clays dispersion and functionalization type.

The final kinetic parameter used to model the degradation process is pre-exponential factor which given the known activation energy and the kinetic model, can be calculated according to Eq. 15³¹.

$$A = -\frac{\beta E}{RT_p^2 f'(\alpha_p)} \exp\left(\frac{E}{RT_p}\right) \quad (15)$$

where $f'(\alpha_p)$ is the differential form of the kinetic model $[df(\alpha)/d\alpha]$, and α_p is the conversion corresponding to the T_{max} . Accordingly, the average values of A were presented in Table 3. As it can be seen, the A value of the filled epoxy systems are much higher than that of pure epoxy because of the presence of clay into epoxy matrix.

With determination of the kinetic parameters, the degradation rate equation for each epoxy systems can be obtained with replacement of its parameters into Eq. 1, which were presented

in Table 4. Moreover, degradation time, t_α , as functions of α and T can be readily determined by Eq. 16 which is integral of Eq. 1³¹:

$$t_\alpha = \frac{g(\alpha)}{A \exp(-E_a / RT)} \quad (16)$$

The obtained equations for degradation time of the epoxy systems were also listed in Table 4.

Table 4 Equations of degradation rate and degradation time as functions of conversion and temperature.

System	Equation of rate degradation	Equation of degradation time
Pure epoxy	$Rate = 6.90 \times 10^{11} \exp\left(-\frac{17320}{T}\right)(1-\alpha)[-\ln(1-\alpha)]^{2/3}$	$t_\alpha = \frac{[-\ln(1-\alpha)]^{1/3}}{2.30 \times 10^{11} \exp\left(-\frac{17320}{T}\right)}$
Epoxy/o-clay	$Rate = 3.01 \times 10^{13} \exp\left(-\frac{19376}{T}\right)(1-\alpha)^{1/2}$	$t_\alpha = \frac{1 - (1-\alpha)^{1/2}}{1.50 \times 10^{13} \exp\left(-\frac{19376}{T}\right)}$
Epoxy/s-clay	$Rate = 17.10 \times 10^{13} \exp\left(-\frac{22840}{T}\right)(1-\alpha)^{2/3}$	$t_\alpha = \frac{1 - (1-\alpha)^{1/3}}{5.70 \times 10^{13} \exp\left(-\frac{22840}{T}\right)}$

3.5. Interpretation of the thermal behaviour

One of the important applications of the equations listed in Table 4 is to predict the usable maximum temperature, the optimum processing temperature regions, and estimated lifetime of the epoxy systems. Also, these equations can be used to interpret the thermal behavior of epoxy systems in relation with its structures. Valuable information can be obtained from analyzing the functions behavior of degradation rate and degradation time in extended temperatures and conversions. For this propose, the logarithmic plots of degradation rate and time were drawn as functions of T and α in Fig. 9. As it can be seen from Fig. 9, degradation rate of the epoxy system containing s-clay is much lower than that of pure epoxy system by 1000 K as well as the o-clay by around 730 K in all conversions. For temperatures higher than 730 K, degradation rate of epoxy/o-clay becomes gradually lower than that of the epoxy/s-clay nanocomposites which strongly depends on its conversion. As the conversion progresses, the surface of degradation rate of epoxy/o-clay at higher temperatures will intersect surface of degradation rate of epoxy/s-clay. It is also interestingly observed that degradation rate of the pure epoxy system is lower than that of the epoxy/o-clay up to 350 K, firmly depending on conversion, and then as the temperature increases, degradation rate of epoxy/o-clay becomes slower, to the point that it even becomes slower than epoxy/s-clay at high temperatures. Since the equations of degradation time is obtained from integral of degradation rate equations, trend in changes of degradation time as functions of temperature and conversion is invers of changes of degradation rate as it is shown in Fig. 9. As it can be

seen, degradation time of epoxy/s-nanoclay is higher than that of the pure epoxy system and epoxy/o-nanoclay at all temperatures and by around 640-870 K, respectively. Beyond this temperature range, degradation time of epoxy/s-clay reduces with respect to the epoxy/o-clay. Additionally, degradation time of epoxy/o-clay at low temperatures is higher than that of the pure epoxy systems only in the low conversions. In other words, at a specific low temperature, more time is required for epoxy/o-clay to reach $\alpha=0.05$ compared to pure epoxy system.

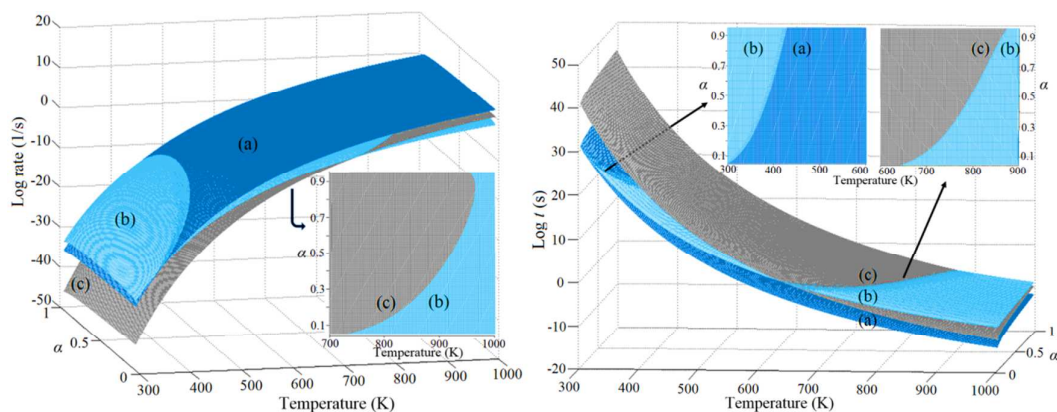


Fig. 9. 3D plots of degradation rate (left) and degradation time (right) as functions of conversion and temperature for the pure epoxy (a), epoxy/o-clay (b), and epoxy/s-clay (c) systems.

The lifetime is generally defined to be when the degree of degradation reaches 5%³¹. This characteristic of epoxy polymers is in a direct relation with thermal durability and performance of epoxy. For determination of lifetime of the epoxy systems, $\alpha=0.05$ should be properly replaced in the equations of degradation time. Fig. 10 illustrates logarithm curves of lifetime of the epoxy systems versus temperature. Interesting findings can be observed from the comparison of changing the trend of lifetime for the epoxy systems. As it can be seen, lifetime of epoxy/s-clay is higher than that of the epoxy/o-clay by 640 K and after that lifetime of epoxy/o-clay exceeds the lifetime of epoxy/s-clay. This means that at the high temperatures, epoxy/o-clay has better thermal performance compared to epoxy/s-clay. It is also observed that at low temperatures, lifetime of pure epoxy system is slightly lower than the epoxy/o-clay and that its lifetime gradually becomes much shorter as the temperature increases. In other words, thermal durability of epoxy/s-clay at low and medium temperatures (below 640 K) is higher than that of epoxy/o-clay and it deteriorates at high temperatures. This behavior at low temperatures may be due to the additional time required to degrade the covalent bonds of s-clay with epoxy matrix in addition to the time for degradation of bonds of epoxy matrix itself. At high temperatures, dissociation of the covalent bonds of s-clay with

epoxy matrix become easier and the effect of thermal diffusion rate is highlighted to determine the lifetime of epoxy systems, so that lifetime of epoxy/s-clay decreases at high temperatures compared to epoxy/o-clay due to the lower thermal diffusion rate of epoxy/o-clay. Based on the calculation presented above, the lifetime of epoxy/s-clay, epoxy/o-clay, and pure epoxy systems at 373K were estimated to be 3.69×10^3 , 7.50 and 1.94 years, respectively.

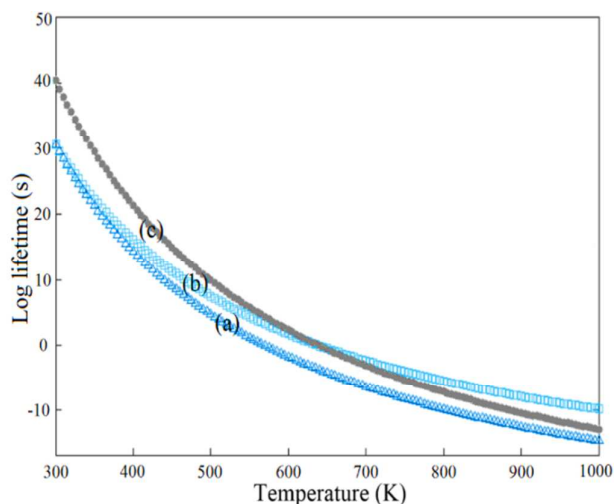


Fig. 10. Logarithm of lifetime as functions of temperature for the pure epoxy (a), epoxy/o-clay (b), and epoxy/s-clay (c) systems.

4. Conclusions

In summary, we investigated the effect of covalent and non-covalent bonding of clay with epoxy matrix on thermal behavior of epoxy and its nanocomposites. The higher values of ΔH_T , T_g and T_{max} suggest that the best thermal properties is achieved for epoxy nanocomposites containing 2% clay. Dependency of degradation activation energy of epoxy nanocomposites on conversion degree confirmed that trend of activation energy does not change since the same loading of clay has been incorporated into epoxy matrix. Nevertheless, its values differ due to the covalent and non-covalent bonding of clay with epoxy matrix. The R_n models with different orders, described as phase boundary controlled reactions, were obtained for kinetic model of phenomenological degradation process of epoxy nanocomposites using fitting method of Criado. According to the R_n model, epoxy/o-clay shows higher order for degradation compared to epoxy/s-clay. This is attributed to the more difficult heat diffusion into epoxy/o-clay which is due to the intercalation of o-clay into epoxy matrix. This is in contrast with s-clay where there are more exfoliated regions in the structure. Investigation of lifetime for epoxy and its nanocomposites revealed that for some applications where low to medium temperatures is required the epoxy/s-clay offers better thermal durability compared to epoxy/s-clay.

Acknowledgment

Deakin University Postgraduate Research Scholarship (DUPRS) awarded to the first author is acknowledged.

References

1. N. Rasoldier, X. Colin, J. Verdu, M. Bocquet, L. Olivier, L. Chocinski-Arnault and M. C. Lafarie-Frenot, *Composites Part A: Applied Science and Manufacturing*, 2008, **39**, 1522-1529.
2. K. Chung, J. C. Seferis and J. D. Nam, *Composites Part A: Applied Science and Manufacturing*, 2000, **31**, 945-957.
3. P. Le Gac, D. Choqueuse, D. Melot, B. Melve and L. Meniconi, *Polymer Testing*, 2014, **34**, 168-174.
4. C. Kit Yan, T. S. Dillon and C. K. Kwong, *Industrial Informatics, IEEE Transactions on*, 2011, **7**, 148-158.
5. J. Hinkley and J. Connell, in *Long-Term Durability of Polymeric Matrix Composites*, eds. K. V. Pochiraju, G. P. Tandon and G. A. Schoeppner, Springer US, 2012, pp. 1-37.
6. K. Pochiraju, in *Long-Term Durability of Polymeric Matrix Composites*, eds. K. V. Pochiraju, G. P. Tandon and G. A. Schoeppner, Springer US, 2012, pp. 383-425.
7. R. Hardis, J. L. P. Jessop, F. E. Peters and M. R. Kessler, *Composites Part A: Applied Science and Manufacturing*, 2013, **49**, 100-108.
8. P. E. Sánchez-Jiménez, L. A. Pérez-Maqueda, A. Perejón and J. M. Criado, *The Journal of Physical Chemistry C*, 2012, **116**, 11797-11807.
9. W. Rmili, M. P. Deffarges, F. Chalon, Z. Ma and R. Leroy, *Journal of Elec Materi*, 2014, **43**, 702-707.
10. A. P. Kumar, D. Depan, N. Singh Tomer and R. P. Singh, *Progress in Polymer Science*, 2009, **34**, 479-515.
11. A. A. Azeez, K. Y. Rhee, S. J. Park and D. Hui, *Composites Part B: Engineering*, 2013, **45**, 308-320.
12. W. Zhang, X. Li and R. Yang, *Journal of Applied Polymer Science*, 2013, **130**, 4119-4128.
13. T. Ahamad and S. Alshehri, *J Therm Anal Calorim*, 2013, **111**, 445-451.
14. J. W. Gilman, *Applied Clay Science*, 1999, **15**, 31-49.
15. Y. Kojima, A. Usuki, M. Kawasumi, A. Okada, Y. Fukushima, T. Kurauchi and O. Kamigaito, *Journal of Materials Research*, 1993, **8**, 1185-1189.
16. K. Wang, L. Chen, J. Wu, M. L. Toh, C. He and A. F. Yee, *Macromolecules*, 2005, **38**, 788-800.
17. T. Lan and T. J. Pinnavaia, *Chemistry of Materials*, 1994, **6**, 2216-2219.
18. P. Kiliaris and C. D. Papispyrides, *Progress in Polymer Science*, 2010, **35**, 902-958.
19. E. P. Giannelis, *Advanced Materials*, 1996, **8**, 29-35.
20. O. Becker, Y.-B. Cheng, R. J. Varley and G. P. Simon, *Macromolecules*, 2003, **36**, 1616-1625.
21. J.-J. Lin, Y.-N. Chan and Y.-F. Lan, *Materials*, 2010, **3**, 2588-2605.
22. P. I. Xidas and K. S. Triantafyllidis, *European Polymer Journal*, 2010, **46**, 404-417.
23. C.-W. Chiu, W.-T. Cheng, Y.-P. Wang and J.-J. Lin, *Industrial & Engineering Chemistry Research*, 2007, **46**, 7384-7388.
24. K. Wang, L. Wang, J. Wu, L. Chen and C. He, *Langmuir*, 2005, **21**, 3613-3618.
25. A. N. Bruce, D. Lieber, I. Hua and J. A. Howarter, *Journal of Colloid and Interface Science*, 2014, **419**, 73-78.
26. M. Huskić, M. Žigon and M. Ivanković, *Applied Clay Science*, 2013, **85**, 109-115.
27. L. Yang, S. L. Phua, J. K. H. Teo, C. L. Toh, S. K. Lau, J. Ma and X. Lu, *ACS Applied Materials & Interfaces*, 2011, **3**, 3026-3032.
28. Y.-N. Chan, R.-S. Hsu and J.-J. Lin, *The Journal of Physical Chemistry C*, 2010, **114**, 10373-10378.
29. C.-W. Chiu, T.-K. Huang, Y.-C. Wang, B. G. Alamani and J.-J. Lin, *Progress in Polymer Science*, 2014, **39**, 443-485.
30. C.-W. Chiu and J.-J. Lin, *Progress in Polymer Science*, 2012, **37**, 406-444.
31. S. Vyazovkin, A. K. Burnham, J. M. Criado, L. A. Pérez-Maqueda, C. Popescu and N. Sbirrazzuoli, *Thermochimica Acta*, 2011, **520**, 1-19.

32. S. Vyazovkin, K. Chrissafis, M. L. Di Lorenzo, N. Koga, M. Pijolat, B. Roduit, N. Sbirrazzuoli and J. J. Suñol, *Thermochimica Acta*, 2014, **590**, 1-23.
33. S. Vyazovkin and N. Sbirrazzuoli, *Macromolecular Rapid Communications*, 2006, **27**, 1515-1532.
34. G. I. Senum and R. T. Yang, *Journal of Thermal Analysis*, 1977, **11**, 445-447.
35. S. Subramani, S.-W. Choi, J.-Y. Lee and J. H. Kim, *Polymer*, 2007, **48**, 4691-4703.
36. Negrete, J.-M. Letoffe, J.-L. Putaux, L. David and E. Bourgeat-Lami, *Langmuir*, 2004, **20**, 1564-1571.
37. R. S. C. Woo, H. Zhu, M. M. K. Chow, C. K. Y. Leung and J.-K. Kim, *Composites Science and Technology*, 2008, **68**, 2828-2836.
38. K. S. Triantafyllidis, P. C. LeBaron, I. Park and T. J. Pinnavaia, *Chemistry of Materials*, 2006, **18**, 4393-4398.
39. P. Vijayan P, D. Puglia, H. J. Maria, J. M. Kenny and S. Thomas, *RSC Advances*, 2013, **3**, 24634-24643.
40. Z. Peng, S.-D. Li, M.-F. Huang, K. Xu, C. Wang, P.-W. Li and X.-G. Chen, *Journal of Applied Polymer Science*, 2002, **85**, 2952-2955.
41. H. E. Kissinger, *Analytical Chemistry*, 1957, **29**, 1702-1706.
42. H. L. Friedman, *Journal of Macromolecular Science: Part A - Chemistry*, 1967, **1**, 57-79.
43. J. M. Criado, J. Málek and A. Ortega, *Thermochimica Acta*, 1989, **147**, 377-385.
44. J. Málek, *Thermochimica Acta*, 1992, **200**, 257-269.
45. B.-D. Park and H.-W. Jeong, *Journal of Industrial and Engineering Chemistry*, 2010, **16**, 375-379.
46. L. Barral, J. Cano, J. López, I. López-Bueno, P. Nogueira, C. Ramírez and M. J. Abad, *J Therm Anal Calorim*, 1999, **55**, 37-45.